Stretchable, flexible, rollable, and adherable polarization volume grating film

KUN YIN, YUN-HAN LEE, ZIQIAN HE, AND SHIN-TSON WU[*]

CREOL, The College of Optics and Photonics, University of Central Florida, Orlando, Florida 32816, USA
[*]*swu@creol.ucf.edu*

Abstract: Volume Bragg gratings (VBGs) have many applications, including filters, wavelength multiplexing devices, and see-through displays. As a kind of VBGs, polarization volume gratings (PVGs) based on liquid crystal polymer have the advantages of nearly 100% efficiency, large deflection angle, and high polarization selectivity. However, previous reports regarding PVGs did not address high efficiency, tunable periodicity, and flexibility. Here, we report a stretchable, flexible, and rollable PVG film with high diffraction efficiency. The control of PVG by mechanical stretching is investigated, while the Bragg reflection band shift is evaluated quantitatively. Moreover, we quantified the deflection angle change's behavior, which has promising potential for laser beam steering applications. The mechanical robustness under stretch-release cycles is also scrutinized.

1. Introduction

Diffraction gratings are dispersive optical elements with periodic index modulations, generally classified into thin gratings (Raman-Nath regime diffraction) and volume gratings (Bragg regime diffraction) [1]. The most representative of these two kinds of gratings are surface relief gratings and holographic volume gratings. Owing to the ability to split and diffract light into different directions, these gratings are widely used in grating couplers [2], spectrometers [3], waveguides [4] and monochromators [5].

Due to interference, volume Bragg gratings (VBGs) exhibit stronger selectivity than Raman-Nath gratings in incident angles and wavelengths. More specifically, VBGs show a relatively small change in both incident angle and wavelength [1]. With proper organization, VBGs can achieve nearly 100% diffraction efficiency at designed wavelength. Ascribed to these unique properties, VBGs are particularly useful for filters, wavelength multiplexing devices and see-through displays [6].

As a kind of high efficiency and large diffraction angle VBGs, liquid crystal (LC) polarization volume gratings (PVGs) shed new light on a unique molecular orientation profile. Following two-dimensional (2D) patterned substrates, the chiral molecules promote self-organization of bulk LC and an asymmetric helical structure can be formed [7]. This results in high-efficiency gratings with unique polarization selectivity where only light with the same chirality as the helical structure will be diffracted by the self-organized grating. Compared to conventional VBGs, such as holographic volume gratings, PVGs achieve nearly 100% first-order efficiency at a very large diffraction angle, and moreover they only respond to certain circularly polarized light. The development of reflective PVGs based on LC materials possesses unique advantages and potentials in diverse areas such as laser beam steering, optical communication systems and waveguide based augmented reality displays [7–12].

Besides distinctive optical features, the elasticity of LC polymers [13–16] grants stretchability and flexibility to LC-based devices [17], particularly intriguing for soft robotics, sensing and biomedical science. The elasticity also hints the potential for changing periodicity of diffractive optical elements, allowing the precise control of diffraction angle and Bragg

wavelength. This property will be beneficial for sensing, spectroscopy and filters, etc [18,19]. However, with only limited examples of tunable VBGs achieved by mechanical strain [20], large-angle, high-efficiency, stretchable, flexible and rollable PVGs have not been reported, to the best of our knowledge.

Although LC polymer itself exhibits elasticity to some extent, achieving good repeatability especially for a very thin polymer layer is still challenging. Here, we demonstrate that with the help of elastic substrates possessing good stretchability, flexibility, chemical stability and reasonable transparency, such as Polydimethylsiloxane (PDMS) [21–23], a stretchable, flexible and rollable LC PVG is achieved. Through characterizing the elasto-optic properties, our stretchable PVG reveals a tunable periodicity with high diffraction efficiency and good repeatability. Moreover, the good adhesiveness of PDMS films enables the volume grating structure to adhere to the surface of glass or other suitable materials [24].

2. Fabrication of PVG film

To create 2D pattern on substrates, brilliant yellow (0.4 wt%) dissolved in dimethylformamide (DMF) [25] was spin-coated onto a clean glass substrate at 800 rpm for 5 s and then 3,000 rpm for 30 s as photo-alignment layer. The substrate was then exposed on two-beam interferometer (λ = 457 nm) with one beam being left-handed circularly polarized (LCP) and the other being right-handed circularly polarized (RCP). The angle between two beams was set at 40°. The PVG precursor consisting of 2.4 wt% chiral agent R5011 (HCCH, helical twisting power HTP $\approx$108 μm^{-1}), 5 wt% initiator Irgacure 651 and 92.6 wt% photo-curable monomer RM257 (HCCH) was diluted in toluene. The precursor was spin-coated onto the exposed substrates then cured with UV light in nitrogen environment. A thin film of PVG was formed on glass substrate. PDMS was prepared by mixing Sylgard 184 Silicone Elastomer with the curing agent at 10:1 ratio [23] followed by 30 minutes of degassing in vacuum chamber. The prepared PDMS precursor was spin-coated onto the PVG and cured for 4 minutes at 110 °C to create smooth and uniform film. Due to the comparatively high affinity of PVG to PDMS, both films can be detached from the glass substrate and a flexible PVG on PDMS was obtained.

3. Results and discussions

3.1 Samples and periodicity measurement

As Fig. 1 illustrates, in the regions exposed by interferometer, the LC directors self-organize into PVGs (red region) [26]. For the unexposed area (yellow region), no in-plane periodicity was defined, and thus uniform symmetric helix was formed, like a regular cholesteric texture.
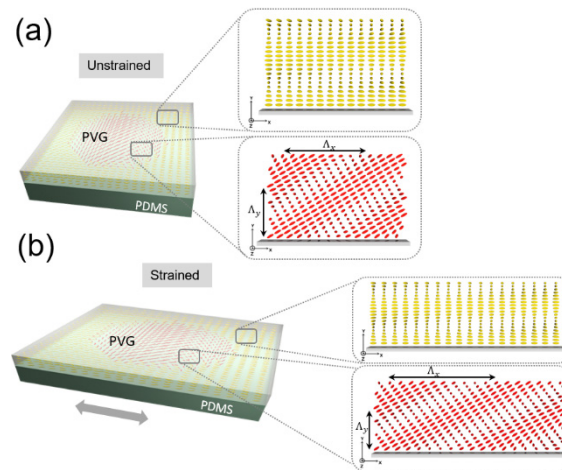
Fig. 1. Schematic illustrations of PVG structure and stretching process of PVG from unstrained state to strained state. (a) PVG on PDMS without strain. (b) Strained PVG structure.

Figure 2 shows three photographs taken at 50° polar angle, showing the deflection and the flexibility of a 3-µm-thick PVG fabricated on a 160-µm-thick PDMS substrate. At this specific angle, the diffracted light from PVG appeared blue. Then we rolled the sample to a radius of curvature of 3.3 mm, as Fig. 2(b) shows. No change in performance was observed, showing good rollability of the flexible PVG structure. Furthermore, the sample can be stretched, bent, and twisted into any shape above this radius. We mount the flexible PVG between a fixed optical stage and a translational optical stage to observe its behavior under strain controlled by the displacement of the precision translational stage (Newport 562-XYZ).
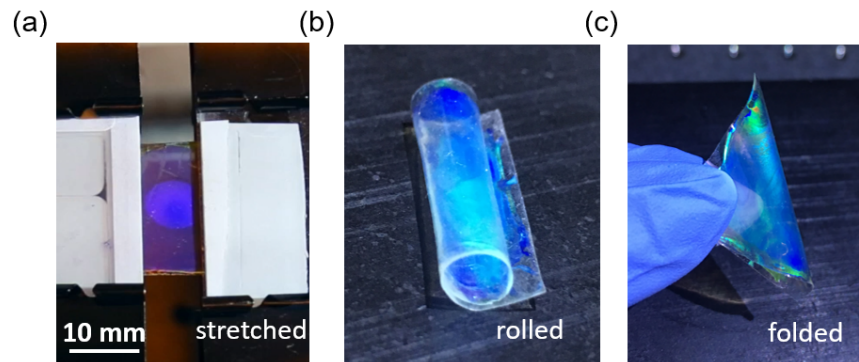

Fig. 2. Images of a 3-µm thick PVG on a 160-µm thick PDMS substrate. (a) To clearly observe the diffraction, sample was viewed under strain. Blue diffraction of PVG is observed in the central area where interference exposure occurred. (b) Rolled sample with a radius of curvature of 3.3 mm. (c) Folded sample.

We first observed the change in horizontal periodicity Λ_x under microscope as depicted in Fig. 3. The initial length of PVG was 6 mm and we increased the stretch length along horizontal direction from 0 mm (initial state) to 2.4 mm. The stretching length from Figs. 3(a) to 3(d) was 0 mm, 1.2 mm, 1.9 mm and 2.4 mm, respectively. During stretching, we found the periodicity gradually changed from 667 nm to 714 nm, 741 nm and 775 nm, confirming that lateral stretch causing the increased horizontal period of PVGs.
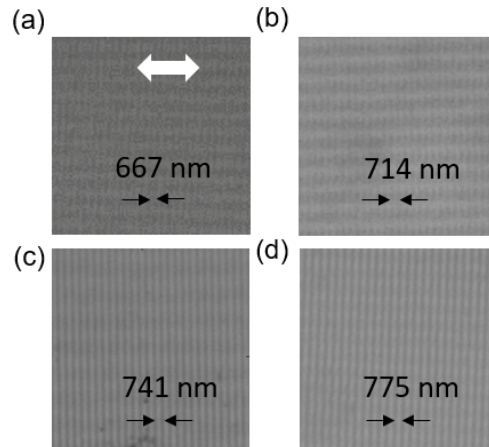
Fig. 3. Optical microscope images of PVG fabricated on PDMS under different strain. The size of each picture is 20 µm x 20 µm and stretching was along the arrow labeled in (a). The periodicity was measured to be: (a) $\Lambda_x \cong 667$ nm (b) $\Lambda_x \cong 714$ nm (c) $\Lambda_x \cong 741$ nm (d) $\Lambda_x \cong 775$ nm.

3.2 Spectrum and diffraction angle

Next, we measured the first-order diffraction efficiency and central wavelength shifting with respect to the applied strain. Results are plotted in Fig. 4. As the stretch length increases, the horizontal periodicity gradually increases and the film thickness decreases, resulting in blueshift of the reflection band and slightly decreased (from 95.1% to 92.7%) diffraction efficiency. Here we recorded 5 points during the strain for spectral analysis as shown in Fig. 4(a). When the stretch length exceeds 2.44 mm, the PVG film approaches its elastic limit. Further stretch would lead to visible cracking of the PVG film. Figure 4(b) depicts the measured central wavelength of transmission spectra as the strain increases. As the strain increases from 0 mm (unstrained) to 2.44 mm (40.6% strain), the central wavelength shifts from 507.5 nm to 474.5 nm, i.e. $\Delta\lambda = 33$ nm. From Fig. 4(b), the blue-shift ($\Delta\lambda$) is approximately linearly proportional to the strain.

The deflection angle of PVG is directly determined by its horizontal periodicity Λ_x, and therefore it is subject to change under strain. The measurement setup was shown in Fig. 4(c). A 532 nm laser diode was used to characterize the change in diffraction angle at normal incidence. Upon diffraction, the beam spot was projected onto a screen set parallel to the probe laser, and from trigonometric relation the first-order diffraction angle was calculated for different applied strain, as shown in Fig. 4(d). The diffraction angle, as expected, decreases at higher strain. As the stretch length increases from 0 mm (unstrained) to 2.44 mm (40.6% strain), the angle changes from 35° to 46.5°, setting the tuning range of 11.5°. The continuous control of diffraction angle holds promising potential for laser beam steering applications. The angle control through strain was recorded in Visualization 1. In addition, the bandwidth of the PVG film is about 25 nm for keeping high diffraction efficiency, as shown in Fig. 4(a). For a fixed incident wavelength, such as 532 nm, the deflection angle has a large tunable range, but the diffraction efficiency will gradually decrease if the Bragg band is shifted far away from the incident wavelength.
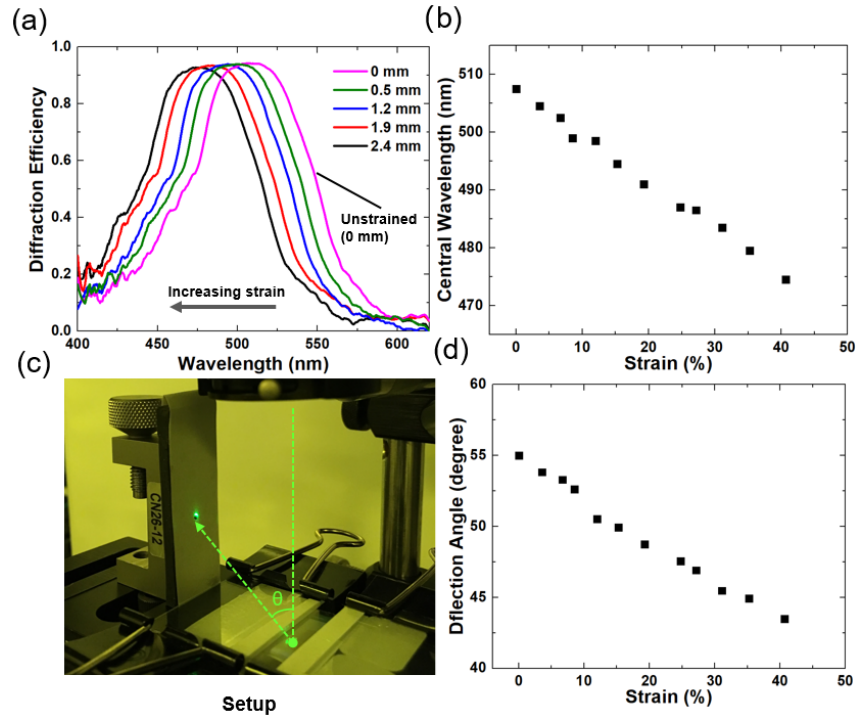
Fig. 4. (a) Measured stretch-induced first-order diffraction spectra and efficiency. Curves from right to left correspond to the stretched length as indicated. (b) Measured central wavelength of diffraction spectra as a function of stretched length, starting from the initial state. (c) Image of experimental setup. The diffraction angle (θ) was marked with green dashed lines (see Visualization 1 for details). (d) Measured diffraction angle at λ = 532 nm under different stretched length, starting from the initial state.

3.3 Theoretical analysis

We also analyzed the changing behavior of Λ_x and Λ_y in stretchable PVGs. Since Λ_x is directly related to the diffraction angle θ, we can calculate Λ_x through:

$$\Lambda_X = \frac{\lambda_{LC}}{\sin\theta}, \tag{1}$$

where λ_{LC} corresponds to the wavelength in liquid crystal. Interestingly, Λ_x is not linearly dependent on the strain, as illustrated in Fig. 5(a). The dependence is fitted by:

$$\frac{\Lambda_X}{\Lambda_{X0}} = (S+1)^a, \tag{2}$$

where Λ_{x0} is the horizontal periodicity without strain, S is the strain and a = 0.49 is a fitting parameter. On the other hand, Λ_y can be determined by:

$$2\Lambda_y \cos^2(\frac{\theta}{2}) = \lambda_B. \tag{3}$$

Combining the measured Bragg central wavelength (λ_B) and diffraction angle, Λ_y can be calculated, as depicted in Fig. 5(b). Λ_y is inversely dependent on the strain and can be fitted by:

$$\frac{\Lambda_y}{\Lambda_{y0}} = (S+1)^{-b}, \tag{4}$$

where Λ_{y0} is the vertical periodicity without strain and $b = 0.49$ is a fitting parameter. We noticed that the two fitting parameters a and b are the same, which ensuring that the product of Λ_x and Λ_y is a constant, as Eq. (5) shows. Similar nonlinear periodicity changes in stretchable LC gels has also been reported [17].

$$\frac{\Lambda_X \Lambda_y}{\Lambda_{X0} \Lambda_{y0}} = (S+1)^{a-b} = 1. \tag{5}$$
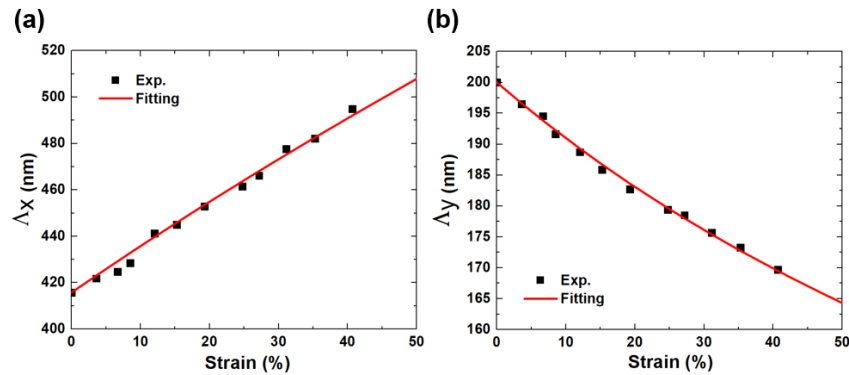

Fig. 5. (a) Derived horizontal periodicity from the measurements and the fitting line with Eq. (2). (b) Derived vertical periodicity from the measurements and the fitting line with Eq. (4).
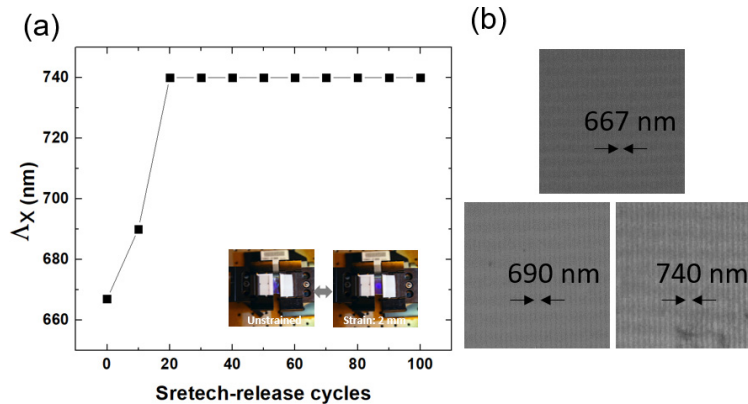
3.4 Robustness test

Fig. 6. (a) Measured horizontal periodicity of PVG as a function of stretch-release cycles, starting from the initial state. Inset: The film was fixed on the electrical holding stages at completely unstrained state. The stretch length was defined by the increased distance between the clamps. Then repeat the stretch-release cycles from unstrained state to 2 mm (see Visualization 2 for details). (b) Optical microscope images of PVG fabricated on PDMS without strain, $\Lambda_{x0} \cong 667$ nm. After 10 stretch-release cycles, $\Lambda_{x10} \cong 690$ nm. And after 20 stretch-release cycles, $\Lambda_{x20} \cong 740$ nm.

To test the mechanical robustness of the stretchable film, we replace the manual translational stage with a precision motorized translational stage (ESP300, Newport) as shown in Fig. 6(a) insert. Before stretching, the film was measured at a periodicity of 667 nm, and then we increased the strain to 33.3% (2 mm stretch length) and released the film, and then repeated

this stretch-release cycle. We measured the periodicity after each 10 cycles. Figure 6(b) shows the optical microscope images with initial state ($\Lambda_{x0} \cong 667$ nm), 10 cycles ($\Lambda_{x10} \cong 690$ nm) and 20 cycles ($\Lambda_{x20} \cong 740$ nm), respectively. After more than 20 stretch-release cycles, we observed a change in periodicity at 0% strain from 667 nm to 740 nm, and yet the PVG on PDMS did not show any crack or wrinkle. This suggests that the PDMS film underwent permanent deformation after 20 cycles but PVG was still within its elastic limit. Further stretching cycles did not change the periodicity at 0%, as shown in Fig. 6(a). Therefore, a pre-strain treatment or a modification in formulation of PDMS was required for better mechanical robustness. The whole process of more than 100 stretch-release cycles was recorded by video (Visualization 2).

4. Potential applications

In this section, we discuss three potential applications of our PVG for laser beam steering [27,28], waveguide coupler in an augmented reality display system, and curved optical element.

4.1 Laser beam steering

As shown in Fig. 4(a), our PVG film has certain bandwidth. For example, if a PVG film is optimized at a central Bragg wavelength $\lambda_B = 507$ nm, without strain its bandwidth is about 25 nm for keeping diffraction efficiency over 90%. In principle, we can optimize the λ_B of our PVG film for a specific wavelength within the entire visible spectrum by controlling the initial periodicity. To prove concept, here we fabricated another sample for laser beam steering at $\lambda_B = 405$ nm. Figure 7 shows the PVG film without strain, in which $\theta = 30°$. As the strain increases, both λ_B and diffraction angle will decrease gradually, as Figs. 4(b) and 4(d) depict.
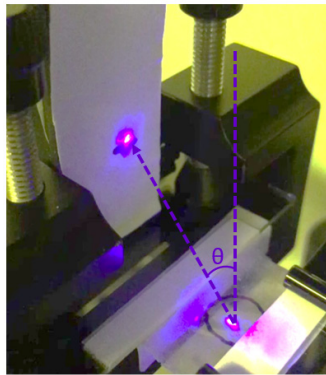

Fig. 7. Image of sample without strain. The diffraction angle (θ) was marked with purple dashed lines. The central wavelength is 405 nm.

4.2 Augmented Reality (AR) waveguide coupler

Compared to conventional volume gratings, PVG film can achieve high efficiency ($\approx$95%) at a large diffraction angle. These optical properties make PVG an excellent candidate for AR optical waveguide couplers. Such a film is quite thin so that it can be easily laminated to a smooth surface, such as planar glass waveguide. Figure 8 illustrates the application of the PVG film in a see-through near-eye system. The light from the display is collimated by optical lenses and then coupled into the waveguide by the PVG film. Based on the total internal reflection (TIR), the incident light propagates in the glass slab and then is coupled out of the waveguide toward human eye. In this system, we can simply adhere the PVG film on the waveguide (glass slab) to replace conventional input and output couplers [29].
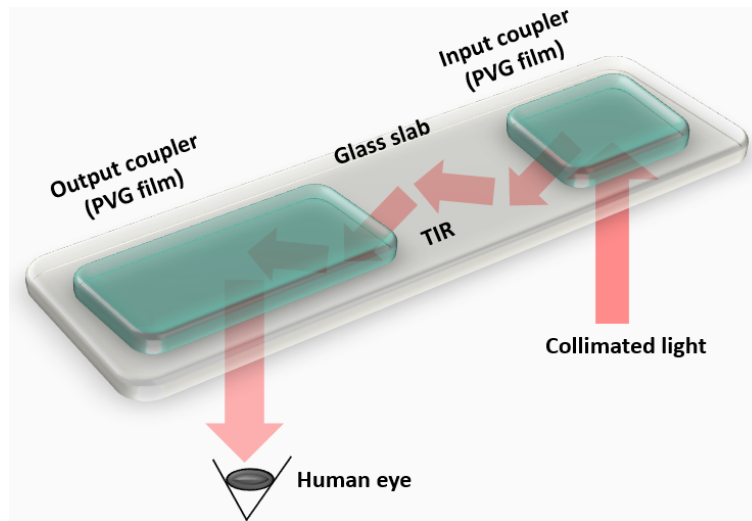
Fig. 8. PVG films used as waveguide couplers in AR see-through near-eye system.

4.3 Curved surface structure

Furthermore, our flexible PVG film can also be laminated onto a curved surface as long as the curvature is not too large, as shown in Fig. 9(a). To demonstrate feasibility, we attached our PVG film on a convex lens whose focal length is 10 cm. No bubble or scattering was observed. As Fig. 9(b) shows, such an integrated optical element combines two functions (collimating lens and input coupler grating) together to achieve a more compact AR system [30]. Moreover, fabricating a uniform optical element on a curved surface is challenging. Our approach provides a new possibility for fabricating PVG or other complex structure on a curved surface.
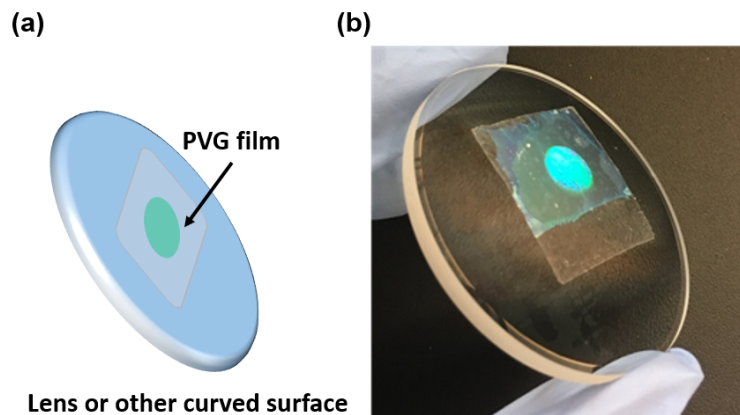

Fig. 9. (a) The concept of combining PVG films with curved surface. (b) The image of lens attached with PVG film.

5. Conclusion

In this paper, we have experimentally demonstrated a stretchable, flexible and adherable PVG based on PDMS substrate with tunable periodicity and high diffraction efficiency. The central wavelength of diffraction spectra shifts from 507.5 nm to 474.5 nm due to the mechanical stretch. The deflection angle can be modulated from 35° to 46.5° with a tuning range of 11°. The flexible PVG has reasonable robustness and can be further improved by chemical

engineering. This thin film opens new possibility for laser beam steering, AR optical systems and fabricating complex structure on a curved surface.

Funding

References

1. T. K. Gaylord and M. G. Moharam, "Thin and thick gratings: terminology clarification," Appl. Opt. **20**(19), 3271–3273 (1981).
2. D. Taillaert, W. Bogaerts, P. Bienstman, T. F. Krauss, P. Van Daele, I. Moerman, S. Verstuyft, K. De Mesel, and R. Baets, "An out-of-plane grating coupler for efficient butt-coupling between compact planar waveguides and single-mode fibers," IEEE J. Quantum Electron. **38**(7), 949–955 (2002).
3. J. W. den Herder, A. C. Brinkman, S. M. Kahn, G. Branduardi-Raymont, K. Thomsen, H. Aarts, M. Audard, J. V. Bixler, A. J. den Boggende, J. Cottam, and T. Decker, "The reflection grating spectrometer on board XMM-Newton," A&A **365**(1), 7–17 (2001).
4. W. Zhang and J. Yao, "A fully reconfigurable waveguide Bragg grating for programmable photonic signal processing," Nat. Commun. **9**(1), 1396 (2018).
5. R. Follath, "The versatility of collimated plane grating monochromators," Nucl. Instrum. Methods Phys. Res. **467-468**, 418–425 (2001).
6. J. Lumeau, L. B. Glebov, and V. Smirnov, "Tunable narrowband filter based on a combination of Fabry-Perot etalon and volume Bragg grating," Opt. Lett. **31**(16), 2417–2419 (2006).
7. J. Kobashi, H. Yoshida, and M. Ozaki, "Planar optics with patterned chiral liquid crystals," Nat. Photonics **10**(6), 389–392 (2016).
8. J. Kobashi, Y. Mohri, H. Yoshida, and M. Ozaki, "Circularly-polarized, large-angle reflective deflectors based on periodically patterned cholesteric liquid crystals," Opt. Data Process. Storage **3**(1), 61–66 (2017).
9. Y. Weng, D. Xu, Y. Zhang, X. Li, and S. T. Wu, "Polarization volume grating with high efficiency and large diffraction angle," Opt. Express **24**(16), 17746–17759 (2016).
10. Y. H. Lee, K. Yin, and S. T. Wu, "Reflective polarization volume gratings for high efficiency waveguide-coupling augmented reality displays," Opt. Express **25**(22), 27008–27014 (2017).
11. W. Duan, P. Chen, B. Y. Wei, S. J. Ge, X. Liang, W. Hu, and Y. Q. Lu, "Fast-response and high-efficiency optical switch based on dual-frequency liquid crystal polarization grating," Opt. Mater. Express **6**(2), 597–602 (2016).
12. H. Chen, Y. Weng, D. Xu, N. V. Tabiryan, and S. T. Wu, "Beam steering for virtual/augmented reality displays with a cycloidal diffractive waveplate," Opt. Express **24**(7), 7287–7298 (2016).
13. M. Warner and E. M. Terentjev, *Liquid Crystal Elastomers* (Oxford University, 2007).
14. T. J. White and D. J. Broer, "Programmable and adaptive mechanics with liquid crystal polymer networks and elastomers," Nat. Mater. **14**(11), 1087–1098 (2015).
15. I. Kasai, Y. Tanijiri, T. Endo, and H. Ueda, "A practical see-through head mounted display using a holographic optical element," Opt. Rev. **8**(4), 241–244 (2001).
16. D. L. Thomsen, P. Keller, J. Naciri, R. Pink, H. Jeon, D. Shenoy, and B. R. Ratna, "Liquid crystal elastomers with mechanical properties of a muscle," Macromolecules **34**(17), 5868–5875 (2001).
17. F. Castles, S. M. Morris, J. M. C. Hung, M. M. Qasim, A. D. Wright, S. Nosheen, S. S. Choi, B. I. Outram, S. J. Elston, C. Burgess, L. Hill, T. D. Wilkinson, and H. J. Coles, "Stretchable liquid-crystal blue-phase gels," Nat. Mater. **13**(8), 817–821 (2014).
18. G. Babakhanova, T. Turiv, Y. Guo, M. Hendrikx, Q. H. Wei, A. P. H. J. Schenning, D. J. Broer, and O. D. Lavrentovich, "Liquid crystal elastomer coatings with programmed response of surface profile," Nat. Commun. **9**(1), 456 (2018).
19. M. Humar, M. Ravnik, S. Pajk, and I. Muševič, "Electrically tunable liquid crystal optical microresonators," Nat. Photonics **3**(10), 595–600 (2009).
20. H. Finkelmann, S. T. Kim, A. Munoz, P. Palffy-Muhoray, and B. Taheri, "Tunable mirrorless lasing in cholesteric liquid crystalline elastomers," Adv. Mater. **13**(14), 1069–1072 (2001).
21. A. Ryabchun, M. Wegener, Y. Gritsai, and O. Sakhno, "Novel effective approach for the fabrication of PDMS-based elastic volume gratings," Adv. Opt. Mater. **4**(1), 169–176 (2016).
22. F. Wang, S. Jia, Y. Wang, and Z. Tang, "Near-infrared light-controlled tunable grating based on graphene/elastomer composites," Opt. Mater. **76**, 117–124 (2018).
23. Y. Arafat, I. Dutta, and R. Panat, "Super-stretchable metallic interconnects on polymer with a linear strain of up to 100%," Appl. Phys. Lett. **107**(8), 081906 (2015).
24. M. J. Tang, P. Chen, W. L. Zhang, A. M. Tam, V. G. Chigrinov, W. Hu, and Y. Q. Lu, "Integrated and reconfigurable optical paths based on stacking optical functional films," Opt. Express **24**(22), 25510–25514 (2016).
25. J. Wang, C. McGinty, J. West, D. Bryant, V. Finnemeyer, R. Reich, S. Berry, H. Clark, O. Yaroshchuk, and P. Bos, "Effects of humidity and surface on photoalignment of brilliant yellow," Liq. Cryst. **44**(5), 863–872 (2017).

26. Y. H. Lee, Z. He, and S. T. Wu, "Optical properties of reflective liquid crystal polarization volume gratings," J. Opt. Soc. Am. B **36**(5), D9–D12 (2019).

27. M. Rafayelyan, G. Tkachenko, and E. Brasselet, "Reflective spin-orbit geometric phase from chiral anisotropic optical media," Phys. Rev. Lett. **116**(25), 253902 (2016).

28. P. Chen, L. L. Ma, W. Duan, J. Chen, S. J. Ge, Z. H. Zhu, M. J. Tang, R. Xu, W. Gao, T. Li, W. Hu, and Y. Q. Lu, "Digitalizing self-assembled chiral superstructures for optical vortex processing," Adv. Mater. **30**(10), 1705865 (2018).

29. Y. Wu, C. P. Chen, L. Zhou, Y. Li, B. Yu, and H. Jin, "Design of see-through near-eye display for presbyopia," Opt. Express **25**(8), 8937–8949 (2017).

30. L. Zhou, C. P. Chen, Y. Wu, Z. Zhang, K. Wang, B. Yu, and Y. Li, "See-through near-eye displays enabling vision correction," Opt. Express **25**(3), 2130–2142 (2017).